Comments on Inorganic Chemistry
Publication details, including instructions for authors and subscription information:
http://www.informaworld.com/smpp/title~content=t713455155

Neutron Scattering: Some Recent Applications to Inorganic Chemistry

Hartmut Fuess[a]
[a] Institut für Kristallographie und Mineralogie der Universität, Federal Republic of Germany

To cite this Article Fuess, Hartmut(1982) 'Neutron Scattering: Some Recent Applications to Inorganic Chemistry', Comments on Inorganic Chemistry, 2: 1, 39 — 67
To link to this Article: DOI: 10.1080/02603598208078109
URL: http://dx.doi.org/10.1080/02603598208078109

Neutron Scattering: Some Recent Applications to Inorganic Chemistry

Structural as well as spectroscopic problems in condensed matter have been investigated by neutron scattering techniques which have proved to be a valuable method for the investigation of chemical problems. Most investigations were performed on crystalline solids, but more and more studies on amorphous material, solutions and adsorbed gases on surfaces are reported. The present article presents examples of structure determination, phase transitions, electron and magnetization densities, together with studies of molecular vibration and other results from neutron spectroscopy.

INTRODUCTION

Neutrons are a unique tool for the study of condensed matter due to their wide range of properties (energy, spin, magnetic moment) (Table I). Research has essentially focused on the properties of the crystalline state. With the advent of high flux beam reactors a large amount of additional work on amorphous material, polymers, solutions and biological substances has been reported. Neutrons with a continuous flux up to 2×10^{15} n cm^{-2} s^{-1} are produced by fission in nuclear reactors. Reactors with fluxes in this range are available at the Institut Laue-Langevin, Grenoble, France, and at Brookhaven and Oak Ridge in the USA. The emitted fast neutrons have to be slowed down by collision with light elements (water, heavy water, carbon) to yield an energy distribution which corresponds to the equilibrium at room temperature (so-called thermal neutrons) with wavelengths between 9.0 and 20.0 nm. This range can be extended by a "hot" source (pyrolitic graphite) to higher energies (shorter wave lengths) or by a "cold source" (liquid

Comments Inorg. Chem.
1982, Vol. 2, Nos. 1–2, pp. 39–67
0260-3594/82/0202-0039/$06.50/0

TABLE I

Properties of the neutron

Mass, $m_0 = 1.675 \times 10^{-24}$g $= 1838.7\ m_e$
Charge = 0
Spin, $s = \pm\frac{1}{2}$
Magnetic moment, $\gamma = 1.913\ e\ h/4\pi m_0\ c = -1.913\mu_N$
μ_N = nuclear magneton

	X rays	Neutrons
Energy in [K]	$h\gamma = hc/\lambda = 1.439 \times 10^7\lambda$	$h^2/2m_0\lambda^2 = 0.949 \times 10^3/\lambda^2$
kT/E (T = 100K, λ = 1.5 Å)	1.04×10^{-5}	2.37×10^{-1}
Interaction	Electromagnetic	Nuclear, magnetic
Wavelength range	Discrete, 0.5–2.28 Å (x-ray tube) Continuous, 0.1–100 Å Synchrotron radiation	Continuous, 0.5–20 Å
Cross section per atom	~100 b	1 b

hydrogen) to lower energies. At present an ultracold source is under construction at the ILL, Grenoble, extending the whole range of neutrons available for scattering experiments to 0.5–100 Å. Figure 1 indicates the wavelength range at present available for neutron scattering experiments. The range covered by synchrotron radiation and by a normal x-ray tube is given for comparison.

A second type of powerful neutron sources is based on a nuclear process termed spallation. An elementary particle (proton or electron) is accelerated by a linear accelerator (LINAC, Rutherford Laboratory, Chilton, UK) or a cyclotron and bombarded onto a target of a heavy element (e.g., lead). The nuclei of the target are excited by the high energy and may return to some fundamental state by losing particles, especially neutrons. The accelerators provide neutron pulses with a maximum of some 10^{17} n cm^{-2} s^{-1} with a very high energy which by moderation are slowed down to the thermal region with fluxes of about 10^{15} n cm^{-2} s^{-1}. The maximum flux is only available for a short period of time; a pulsed neutron source is therefore especially suited for all types of time-of-flight techniques.

Several interactions between the neutron and an atom exist, leading to different scattering processes. The interaction between neutron and

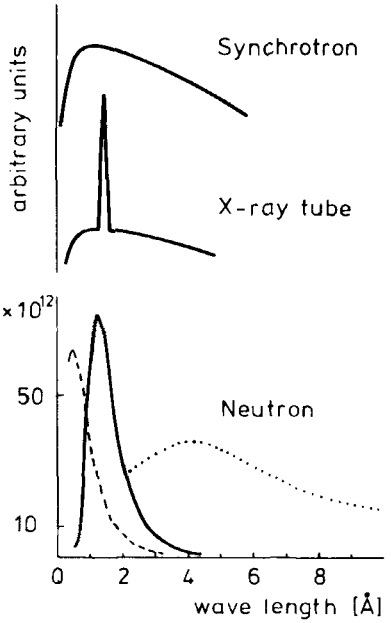

FIGURE 1 The wavelength range available for scattering experiments from the high flux beam reactor (HFBR) of the ILL (below). ___ thermal, _ _ _ _ hot, ... cold neutrons. Intensity in units of neutrons $cm^{-2}s^{-1}$. X-ray wavelength from tube and synchrotron radiation (above). Intensities on arbitrary scale.

an atomic nucleus leads to an intermediate compound which may be altered by an absorption of the neutron or by a reemission of the particle with unchanged energy (elastic scattering or diffraction) or with an energy gain or loss (inelastic scattering). The magnetic scattering is caused by the interaction of the moment of the neutron with unpaired electrons or transition elements. The nuclear scattering is described by the scattering length b (given in units of 1 fm = 10^{-15}m) which is independent of the scattering angle. The magnetic scattering power of an atom is, however, a function of the scattering angle and therefore shows a form-factorlike behavior. Inelastic neutron scattering is possible because the low energy of neutrons is in the same range as an energy change caused by the collision of the particle with an atom in a crystal or molecule. The change is therefore easily detectable.

Neutron scattering studies of interest to chemists fall into the following categories:

Structural studies to answer specific questions like location of light elements or distinction of elements which are adjacent in the periodic table. A combination of neutron and x-ray data is a suitable tool to reveal bonding electrons.

Magnetic structure determination in ferro-, ferri- or antiferromagnetic material and magnetic spin distribution.

The inelastic scattering of neutrons is a spectroscopic method which is complementary to light scattering and is essentially sensitive to the large incoherent scattering of hydrogen.

Some practical aspects of neutron scattering are the following. The absorption cross section of any material for neutrons is less pronounced than for x rays. A wide range of auxiliary equipment (low and high temperature devices, pressure cells) is therefore widely used.

The large difference in the scattering power of H and D leads to a variety of applications based on H/D exchange. More details are given in a book by Bacon[1] and in an extended article on the chemical application of neutrons by the present author.[2] The fundamental theory of neutron scattering was treated by Marshall and Lovesey.[3]

CRYSTAL STRUCTURE DETERMINATION

The profile analysis technique[4,5] in connection with high resolution powder diffraction became increasingly popular over the last decade. This method treats the pattern as a whole without extracting individual structural factors. Its main strength is shown by fitting a group of overlapping reflections with a function that is the sum of individual lines. About 100 parameters may be refined for 1000 lines. A starting model is usually necessary but a complete structure determination on a constrained organic ring system has been reported by Pawley *et al.*[6] The main problems connected with the method are a precise determination of the background level and the correlation between several parameters. In complex patterns only small regions occur where no lines contribute. Profile refinement was quickly adopted for the study of magnetic structures, uranium halides, phase transitions, hydrogen bonding and disordered structures. Mainly inorganic material has been studied, but work on organic molecules became feasible, especially in con-

nection with constrained refinement.[7] Work done prior to 1977 has been reviewed by Cheetham and Taylor.[8]

Hewat[9,10] studied the various phases and phase changes in the ferroelectric material $KNbO_3$. The structural changes are due to small displacements of the atoms from the ideal positions of the high temperature cubic perovskite structure:

$$\text{rhombohedral} \overset{10°C}{\longleftrightarrow} \text{orthorhombic} \overset{225°C}{\longleftrightarrow} \text{tetrahedral} \overset{435°C}{\longleftrightarrow} \text{cubic}.$$

The powder diagrams of the tetragonal and the orthorhombic distorted phase are shown in Figure 2. The common feature of the different phases of $KNbO_3$ is the rigidity of the oxygen tetrahedron. The phase changes occur by a displacement of the metal atoms versus this rigid unit. The displacement of Nb is in the direction [001] in the tetragonal (Figure 2a) along [011] in the orthorhombic (Figure 2b) and along [111] in the rhombohedral phase.

Profile analysis techniques have also been applied to a great number of nonstoichiometric oxides, hydrides and carbides where interesting types of clusters have been detected.[8] The location of hydrogen is one of the classical applications of neutron diffraction. Numerous examples have been reported on hydrogen in metals. For a review see Springer.[11]

A large amount of work has been done on all types of hydrogen bonding which led to a precise knowledge of the geometry of these bonds. For O–H · · · O bonds this knowledge is summarized in Figure 3, which shows the correlation between O–H and O · · · O distances. The curve has been given by Ishikawa,[12] but some recent studies on very short hydrogen bonds (O · · · O distances below 2.45 Å) are included. It seems that in the region of very short H bonds a variety of O–H lengths is possible. For the O · · · O range 2.39 · · · 2.40 eight observations are reported with O–H distances from 1.108 to 1.199 Å. The distance for a "normal," nonhydrogen bonded O–H distance is about 0.98–1.00 Å. Recently a series of papers on transition metal hydride complexes[13] revealed a variety of metal–hydrogen–metal connections. An interstitial hydrogen in a metal cluster was found by Hart *et al.*[14] in $[Ph_3P_2N]^+$ $[HCo_6(CO)_{15}]^-$ where it occupies the center of the CO_6 octahedron (Figure 4). A similar observation was reported for $[Ph_4As]$ $[HRu_6(CO)_{18}]$.[15] Both compounds exhibit unusual ^{1}H-NMR signals. Another interesting result with hydrogen atoms acting as bridges between two rhenium metals is given in Figure 5.[16]

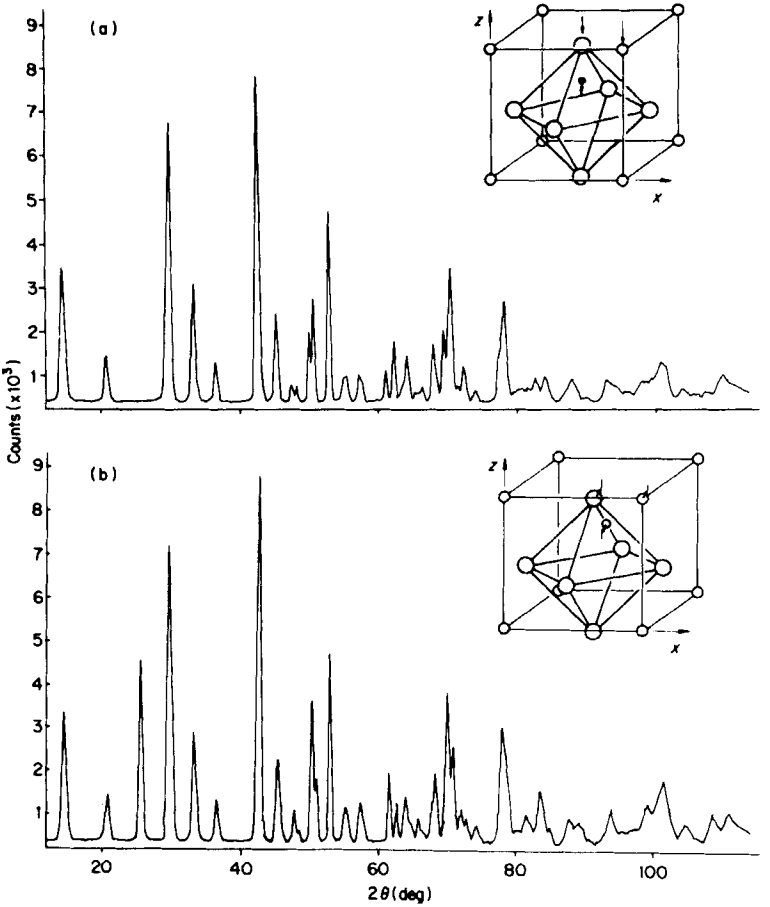

FIGURE 2 Powder diffraction pattern and structure of the (a) orthorhombic, (b) tetragonal phase of $KNbO_3$.

A very unusual application of neutron diffraction was reported by Bacon and his colleagues who studied bones.[17,18] Neutrons offer considerable advantages over x rays because of greatly reduced absorption. The mineral part of bone consists mainly of apatite $Ca_5(PO_4)_3F$ or hydroxy apatite $Ca_5(PO_4)_3OH$ easily distinguishable by neutrons. Samples up to 1 cm can be used and measurements of preferred orientation can

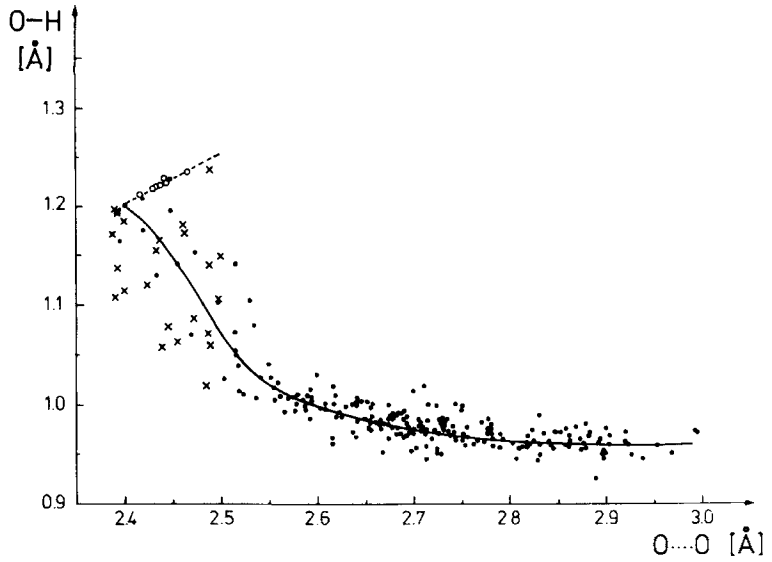

FIGURE 3 Correlation between O–H and O · · · O distances from neutron diffraction studies.

be made and the properties of the bulk material can be studied. Preferred orientation of crystallites in bones is a result of the strength exercised on the bone by the muscle. The crystallites are oriented in such a way as to withstand stress in the most economical way. An additional objective of neutron studies is the connection between collagen and the mineral, reported for a calcified leg tendon by White *et al.*[19] Bacon *et al.*[17] gave results on the chemical nature of the mineral (apatite or hydroxy apatite) and on its texture and crystallite size.

Several experiments have been reported on the formation of intercalate products of dichalkogenide layer structures.[20] The diffusion of small molecules (NH_3, N_2H_4) or the galvanostatic reduction products of 2H-TaS_2 in D_2O/K_2SO_4 were observed by neutron scattering as a function of time. The scattering lengths of N, D, H and S differ considerably and neutrons are therefore well suited to locate organic intercalates. The pyridine orientation (Figure 6a) in TaS_2 and NbS_2 was proposed from x-ray and NMR data. Neutron diffraction on single crystals and powders revealed, however, the model of Figure 6b.[21]

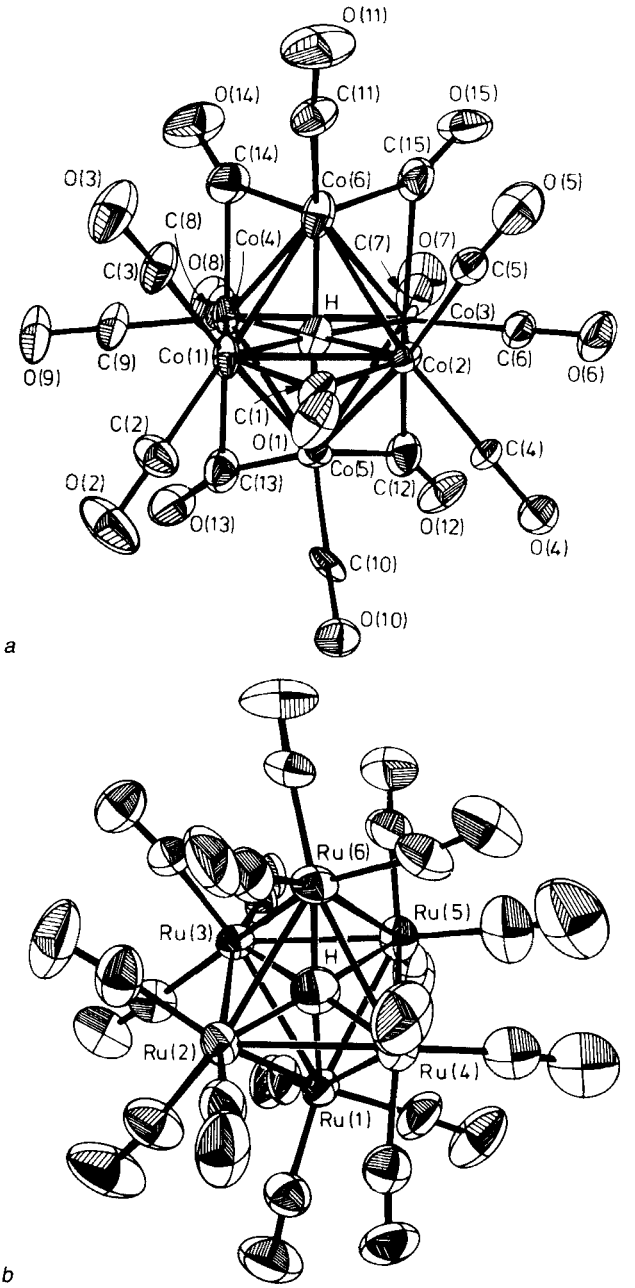

FIGURE 4 (a) A molecular plot of the $HCo_6(CO)_{15}^-$ anion.[14] (b) The structure of the $HRu_6(CO)_{18}$ anion.[15]

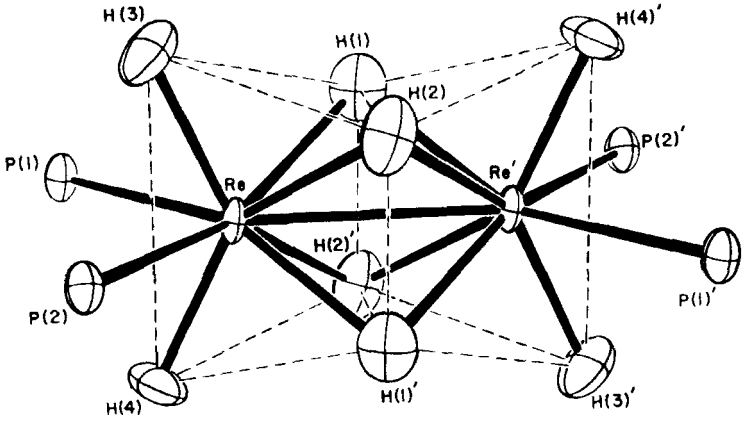

FIGURE 5 The central core of the $H_8Re_2(PEt_2Ph)_4$ molecule.[16]

The reduction of TaS_2 in D_2O/K_2SO_4 was followed as a function of charge transfer, which led to the intercalation of K and D_2O between the layers. First, second and third stage compounds were formed by occupation of every second or third layer. The periodicity in the c direction therefore changed and new 001 reflections of the original phase and of the intermediate phases change considerably as a function of reaction time (Figure 7).[20]

It should be mentioned briefly that neutron scattering techniques contributed considerably to the knowledge of the structure of synthetic polymers and biopolymers. Studies were carried out on crystalline proteins (myoglobin, lysozyme), on solutions of proteins and nucleic acids, on membranes, viruses or ribosomes.

The large difference in the scattering power of hydrogen and deuterium allows a partial labeling of parts of these large units.[22] Furthermore, a continuous variation of the scattering power of an aqueous solvent is possible by H_2O/D_2O mixtures. A full account of the application of neutrons to biology has recently been given.[23]

DEFORMATION AND MAGNETIZATION DENSITIES

The chemical bond in molecules and solids involves the outer electrons of the atoms. A knowledge of the distribution of electrons therefore

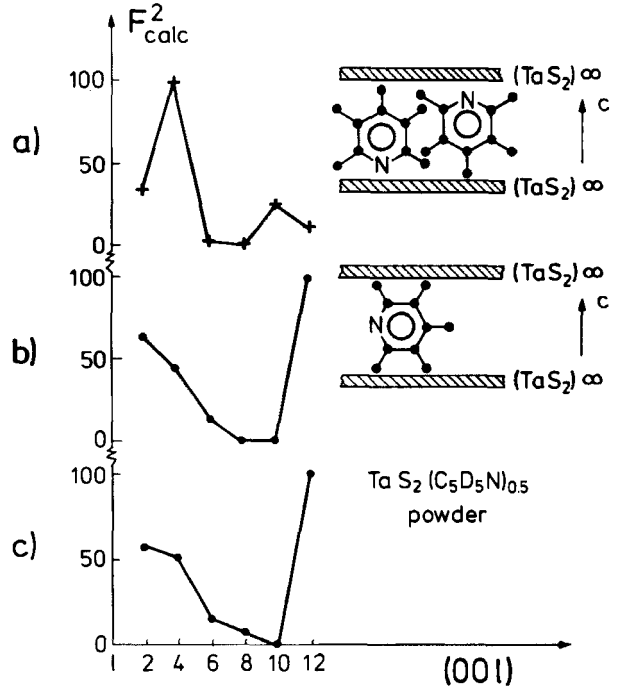

FIGURE 6 (a) Pyridine orientation in $TaS_2(C_5D_5N)_{0.5}$ according to x-ray and NMR data together with calculated neutron F^2 values. (b) Pyridine orientation in $TaS_2(C_5D_5N)_{0.5}$ from neutron powder diffraction data. Calculated F^2 values. (c) Observed F^2 for $TaS_2(C_5D_5N)_{0.5}$ powder after Ref. 20.

gives considerable insight into the nature of the bond. The electron distribution may be studied by x-ray diffraction which is sensitive to all electrons or by neutrons that show only the distribution of magnetic unpaired electrons of d or f shells of transition elements, rare earths or actinides. In addition to the study of the complete distribution of electrons, a difference technique, called X–N or deformation density combines x-ray and neutron results. X-ray analysis reveals the centroid of the electron density distribution around an atom, not the precise position of the nucleus. The coordinates of the atom are therefore somewhat shifted when determined by x rays. The procedure of producing an X–N deformation density includes the following steps:

(a) An accurate x-ray study provides the complete electron distribution.

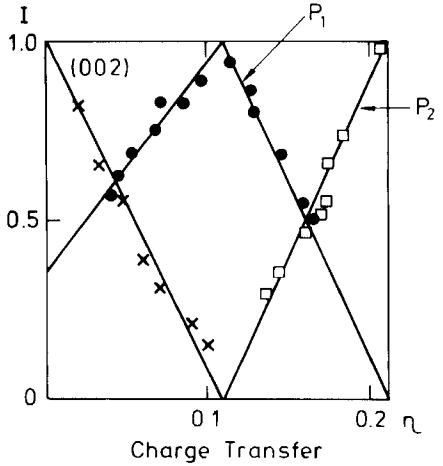

FIGURE 7 Change of intensities of (002) of 2H–TaS_2, intermediate phase reflection P1 and (004) of first stage phase (P2) during $K_x(D_2O)_yTaS_2$ formation[20] as a function of charge transfer.

(b) Neutron diffraction gives accurate positional parameters of the nuclei and their thermal movement.

(c) A density is calculated at the nucleus position with spherical form factors simulating an unbonded free atom.

(d) The difference between steps (a) and (c) is calculated showing all features that are due to bonding. This function is called $\Delta\rho$(X–N) function or X–N density.

Care has to be taken to reduce thermal motion (low temperature studies) and systematic errors. The results are then compared with theoretical calculations based on molecular orbital considerations.

An example for such a comparison is shown in Figure 8 for the formate group in NaHCOO.[24] The peak heights observed for several studies of that group in different compounds are shown in Table II. The agreement between the experimental and theoretical densities is good. Discrepancies are mainly observed in the lone pair region. These differences may result from a possible influence of the Na^+ ion on the charge of the oxygen atom.

The study on H_2O_2[27] has revealed an absence of positive charge density between the oxygen atoms. Large and well defined densities are found in between oxygen and hydrogen (Figure 9). The authors explain the

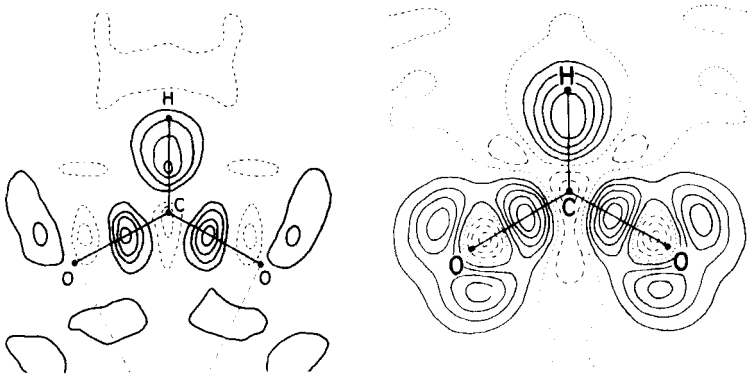

FIGURE 8 Experimental (left) and theoretical deformation density in the formate group of NaHCOO.[24]

absence of electrons between the oxygens by the way of calculating the difference maps. This uncertainty reveals at the same time the ambiguity of the result which seems to depend somewhat on the method applied to treat the data.

The range of O–O lone pair and H–O lone pair angles between 83° and 113.7° shows a distorted tetrahedral environment of the oxygen with the oxygen in a sp^3 configuration. Figure 9c shows a section of the $\Delta\rho$ (X–N) through the atoms O · · · H–O, where the oxygen–hydrogen bond points toward regions of high electron density, which seems to be typical for long hydrogen bonds. Work on short metal–metal contacts which have been termed double or triple bonds did not show any density in the midpoint of the bond.[28]

Neutron diffraction in its own way may be extremely sensitive to covalent bonding when neutrons are polarized. It is possible with this technique to measure small magnetic contributions to a diffracted peak because a ratio is actually determined in a stationary count:

$$R = \frac{I^+}{I^-} = \frac{(F_N + F_M)^2}{(F_N - F_M)^2} = \frac{(1 + \gamma)^2}{(1 - \gamma)^2} \quad \text{with} \quad \gamma = \frac{F_M}{F_N}.$$

R is the ratio of scattered neutrons with the two different spin states. Magnetic contributions down to 1% of the total intensity may easily and accurately be determined. Coincidence of nuclear and magnetic reflections at the same angle is, however, a prerequisite. This coincidence is observed in many metals and alloys which exhibit ferri- or

TABLE II

Peak heights in electron density differences of the formate ion (e Å^{-3})[a]

	Theoretical			Experimental			
Molecular region	α-Ca $(HCOO)_2$ 100 K	NaHCOO 120 K (Ref. 24)	$LiHCOO \cdot H_2O$ 298 K	α-Ca $(HCOO)_2$ 100 K X–N (Ref. 25)	NaHCOO 120 K X–N (Ref. 22)	$LiHCOO \cdot H_2O$ 298 K X–N (Ref. 26)	$LiHCOO \cdot H_2O$ 298 K M–A (Ref. 26)
C–H	0.45	0.45	0.30	0.40	0.45	0.20	0.25
C–O(1)	0.55	0.55	0.35	0.45	0.50	0.25	0.30
C–O(2)	0.55		0.35	0.25	0.50	0.30	0.35
O(1) l.p.	0.45, 0.40	0.45, 0.40	0.35, 0.30	0.30, 0.35	0.20, 0.15	0.10, 0.20	0.20, 0.25
O(2) l.p.	0.45, 0.40		0.30, 0.30	0.45, 0.40	0.20, 0.15	0.15, 0.20	0.15, 0.20

[a]For the labeling of the atom consult Refs. 24,26. l.p. stands for lone pair; the value of the l.p. peak heights refers to the l.p. lobe that is directed towards the C–H bond; M–A stands for multipole deformation density.

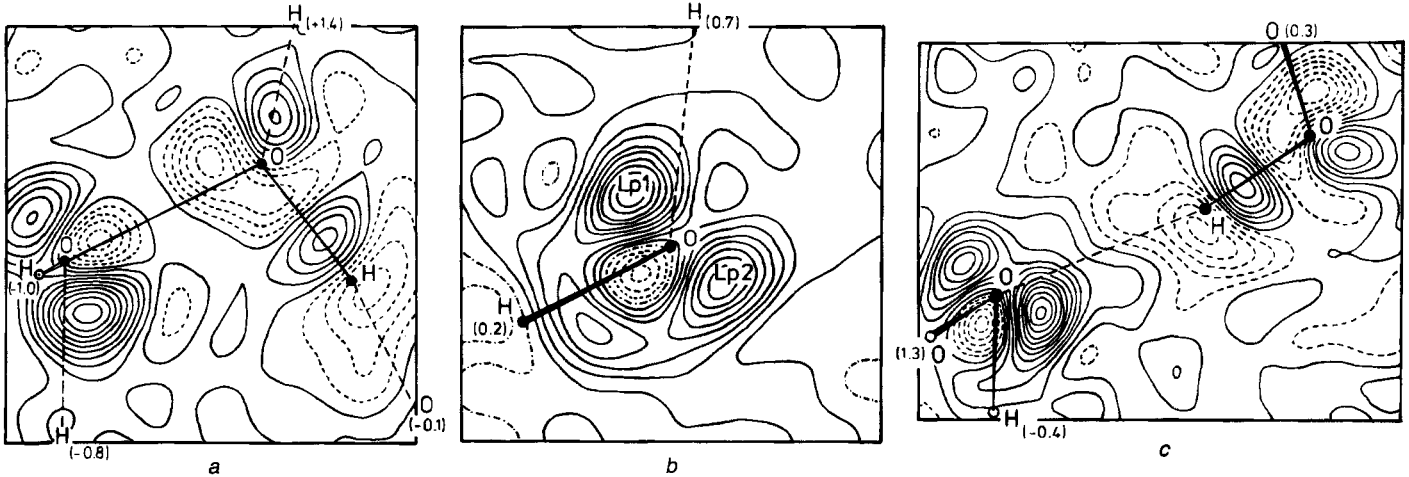

FIGURE 9 Deformation density in H_2O_2. (a) The O–O bond. (b) Section orthogonal to the oxygen–oxygen bond through the oxygen atom. (c) Section through the atoms O · · · H–O involved in the hydrogen bond. Interval between contours 0.1 e Å^{-3}.[27]

ferromagnetic ordering. Relatively few studies of ordered magnetic salts have been made because these usually order antiferromagnetically. Exceptions include the weak canted ferromagnets like $MnCO_3$ in which the spatial distribution of the small ferromagnetic moment has been measured[29] and some ferrimagnetic mixed oxides, like Fe_3O_4[30] and yttrium iron garnet (YIG).[31] The polarized neutron method has also been applied to an organic free radical, namely di(2,2,6,6-tetramethyl-4-piperidinyl-1-oxyl)-suberate. Polarized neutrons elucidated the controversial point of the location of the unpaired spin which was found to be equally distributed between nitrogen and oxygen.[32]

We shall give a few more details on the study of YIG. Fe^{3+} ions occupy a tetrahedral and an octahedral site in the garnet structure. Octahedra and tetrahedra are linked by a common oxygen atom. The magnetization density as determined by polarized neutrons is shown in Figure 10 and reveals a net amount of uncompensated spin on the oxygen atom and in the intermediate region between oxygen and tetrahedral iron, thus giving direct evidence of covalent bonding and illustrating most strikingly the superexchange postulated by Néel's theory of ferrimagnetism. A considerable reduction of the value of the magnetic moment of Fe^{3+} is observed at the same time, a reduction which corresponds to that found in Fe_3O_4.

ABSORPTION ON SURFACES

Surface effects have been studied quite extensively over a long period of time, but the understanding of chemical processes like catalysis is still at a low level. Many of the effects caused by mono- or multilayers of atoms on external or internal surfaces can be observed by optical and other spectroscopic methods. In the spectrum of the substrate there must exist a window in order to allow optical measurements on the absorbed species or reflection techniques have to be used. Due to these restrictions in concurrent methods, neutron scattering offers a unique insight into the intermolecular forces by the measurement of external and internal modes and intramolecular excitations.

The study of adsorbed species on substrate like graphite, metal surfaces or zeolites may be subdivided into diffraction, which gives results on the structure of the adsorbate, and in quasi and inelastic scattering, answering questions on diffusion processes and vibrations. Systems like N_2, Ar, H_2O_2, NO, NH_3 on grafoil or graphon give reasonable signal

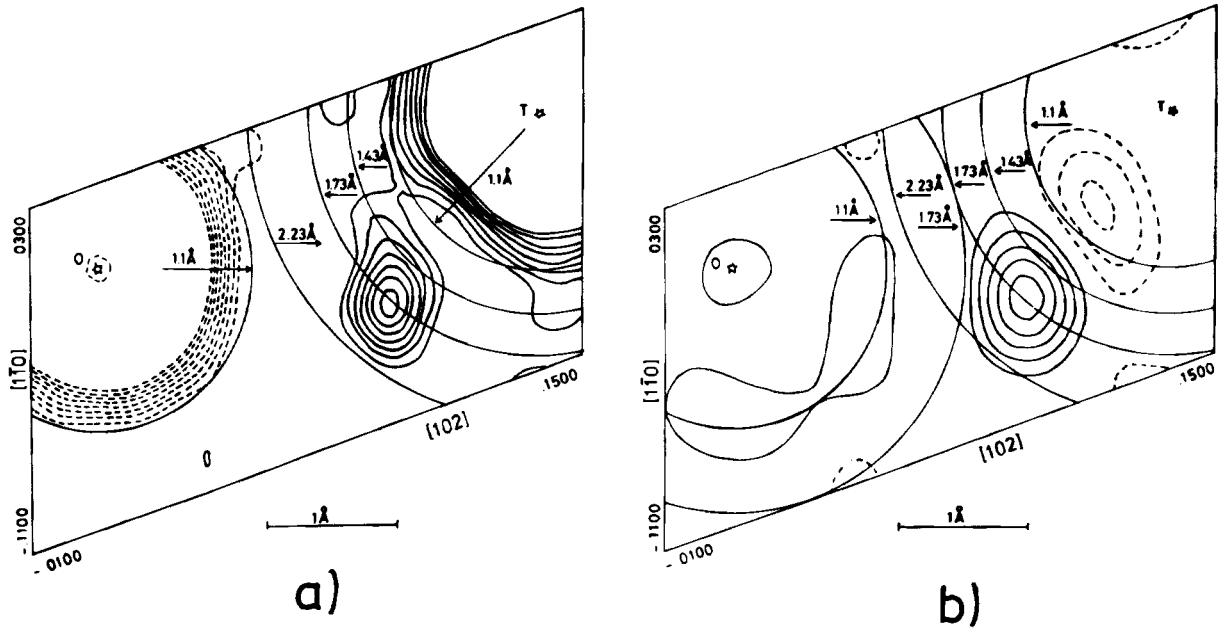

FIGURE 10 (a) Total magnetization density in yttrium iron garnet (YIG). O Position of the octahedral Fe^{3+}, T position of the tetrahedral Fe^{3+} (above). (b) Difference density between the total magnetization density and that due to iron, giving clear evidence of residual moment density on the oxygen and in the bond between the tetrahedral iron and oxygen.[31]

to noise ratios for the diffraction pattern of the adsorbed phase and are appropriate to measure the first few orders of diffraction.[33]

Figure 11 shows the neutron diffraction from one monolayer of nitrogen on grafoil at different temperatures.[34] The size of a two-dimensional unit cell was derived from the 2θ position and gives a $\sqrt{3} \times \sqrt{3}$ structure in registry with the graphite basal plane. The intermolecular spacing of the adsorbed nitrogen is larger than that determined by diffraction on bulk liquid nitrogen at 78 K (Figure 11a). Further addition of nitrogen gas left the peak almost unchanged until a little over one monolayer had been completed. Further addition of N_2 resulted in a

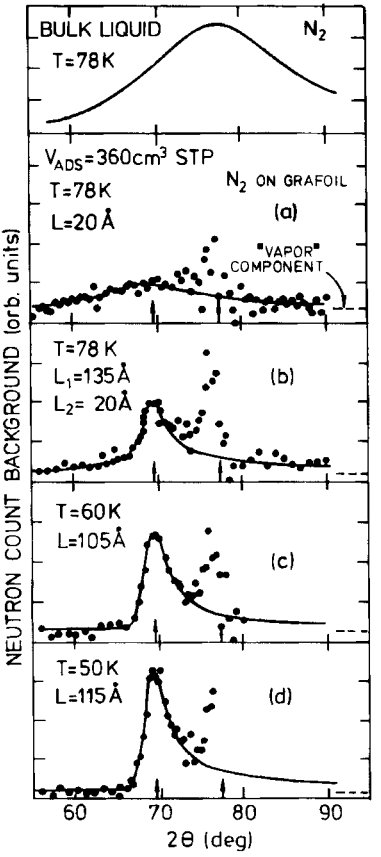

FIGURE 11 Neutron diffraction from one monolayer of nitrogen on grafoil at different temperatures compared with the diffraction pattern for liquid nitrogen at 78 K.[33,34]

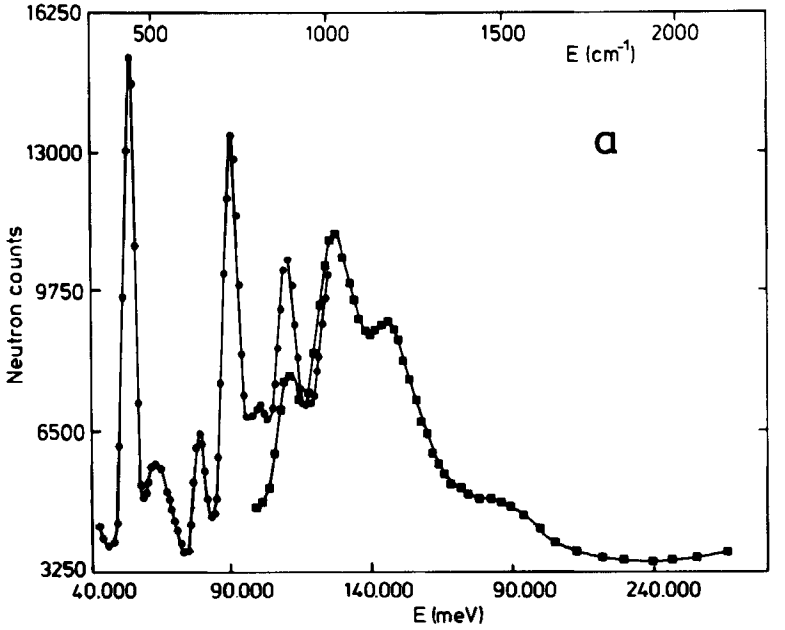

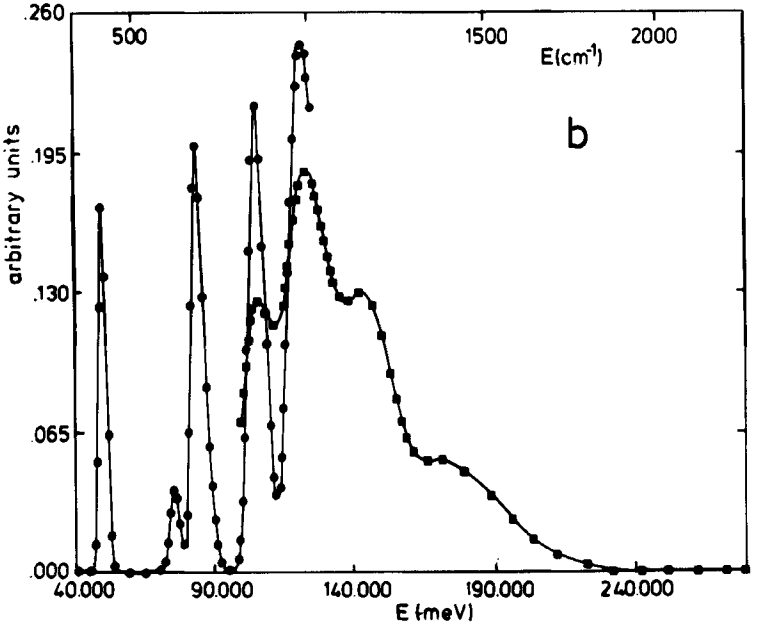

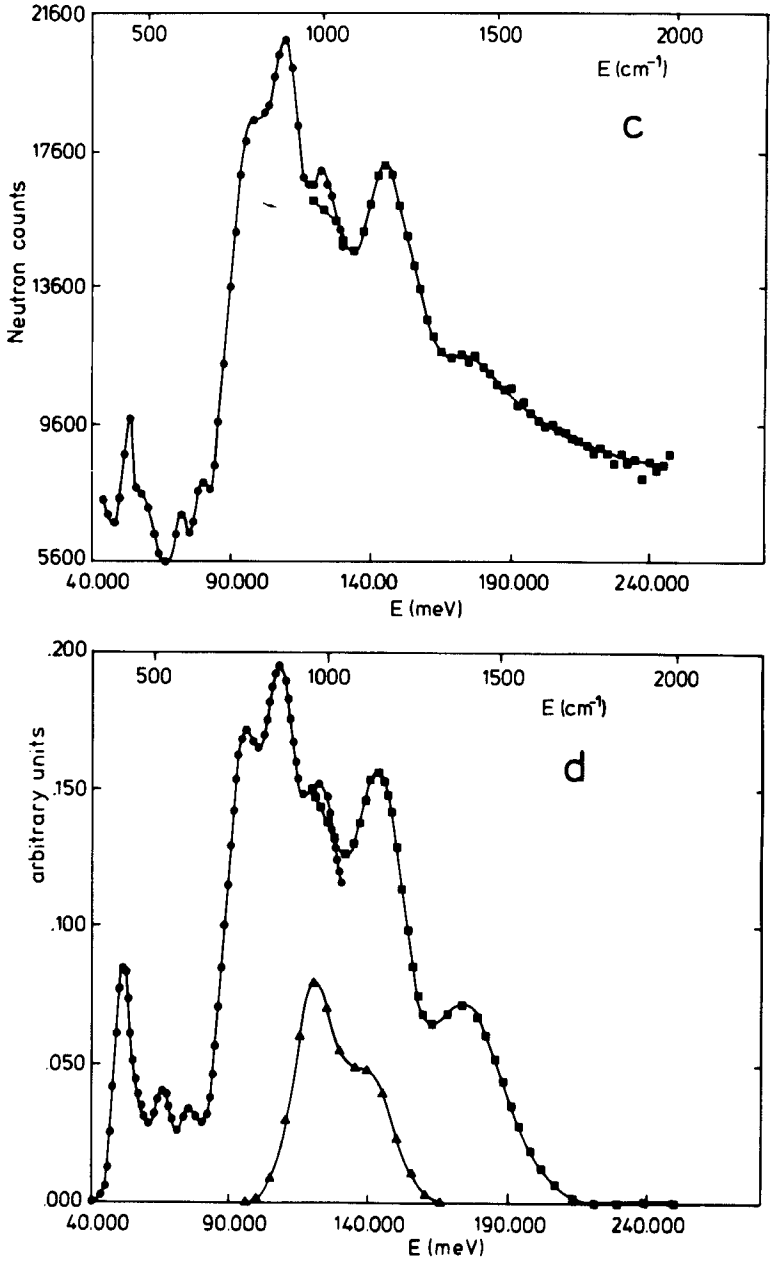

FIGURE 12 (a) Observed neutron spectrum of solid benzene. (b) Calculated spectrum for benzene after Ref. 35. (c) Observed neutron spectrum of adsorbed benzene on Raney nickel (77K). (d) Calculated spectrum for adsorbed benzene with added experimental spectrum of adsorbed hydrogen.

progressive development of a peak at $2\theta \approx 70°$ below 50 K. Finally, the peak associated with the $\sqrt{3} \times \sqrt{3}$ structure disappeared by completion of the second layer. The peak shift to higher scattering angles indicates that the nitrogen molecules pack more closely by formation of a second layer.

Catalytic hydrogenation of benzene on transition metals is a model reaction. We have therefore chosen the vibrational spectrum of benzene on Raney nickel as an example of inelastic neutron scattering of an adsorbed species.[35] The experimental spectrum is compared to that of benzene at 77 K and to a theoretically calculated one. The theoretical one (Figure 12d) has been calculated from a force field which was derived from the study of a model substance (benzenetricarbonylchromium) by changing a few force constants. The authors obtain good agreement if they add to the calculated spectrum the contribution from chemisorbed hydrogen. The strong perturbation of the adsorbed molecule leads to weakening of the C–C stretching force constant. This weakening was derived by comparison with the frequencies observed in free benzene. It was concluded from the results that benzene lies flat on the metal surface and is preferentially bound to one nickel atom, at a distance of 2.5 ± 0.5 Å in general agreement with data on benzene adsorbed on single crystal (111) and (100) faces obtained by LEED and energy loss spectroscopy (ELS).

STRUCTURE OF SOLUTIONS

The structure of liquids, amorphous material and solutions is generally described as short-range order. The three-dimensional periodicity in crystalline solids no longer exists and the structure is described by a probability of finding an atom at a time $t = 0$ at a position $r = 0$ when a monoatomic system is considered. The corresponding function is the pair distribution function $g(r,t)$ which is derived by Fourier transform from the liquid structure factor that is experimentally accessible. The general approach is to measure the scattering cross section per unit solid angle and energy. In the static approximation from which structural aspects are derived, a pattern is obtained with a strong first order peak followed by several weaker peaks of higher order (Figure 13). Short wavelengths are preferred in order to extend the spectrum to higher scattering angles or Q ranges ($Q = 4\pi \sin\theta/\lambda$). For further experimental details see Chieux.[36]

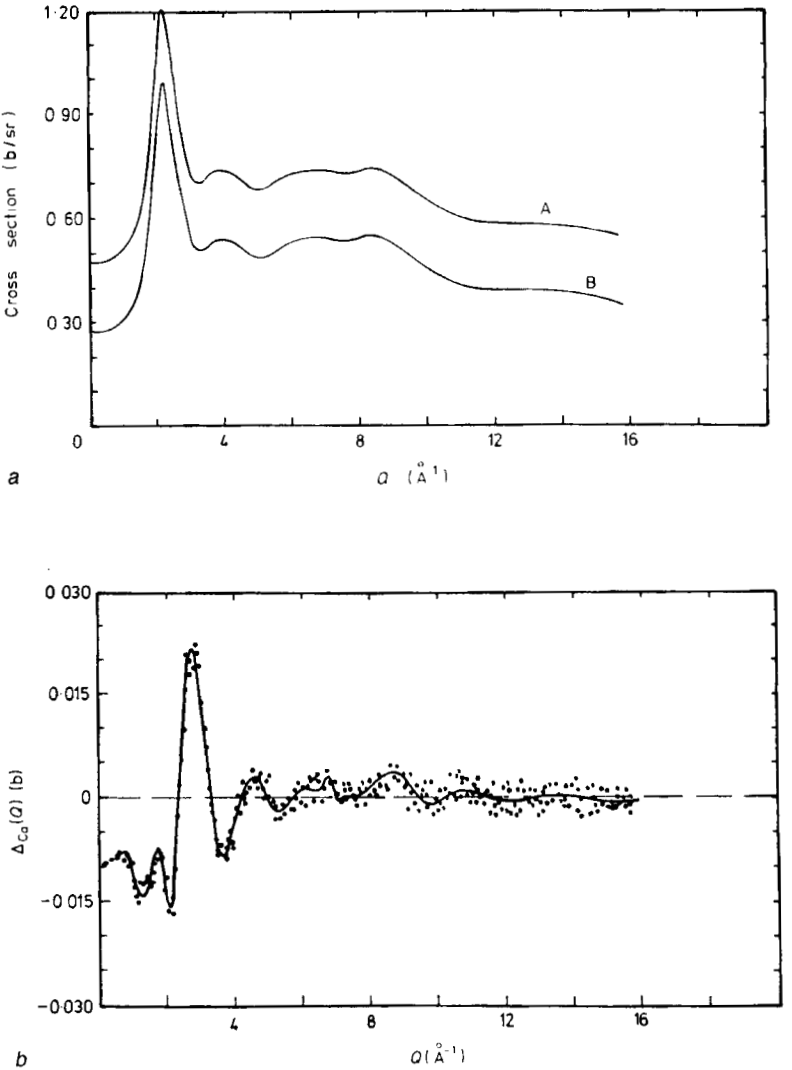

FIGURE 13 (a) Scattering for two Ca-substituted solutions of $CaCl_2$ in D_2O : (A) $^{44}CaCl_2$ (B) $CaCl_2$ with Ca in natural abundance. (b) The difference between the two curves shown in (a). The full circles are experimental points and the smooth curve is the one used to calculate the pair correlation function.[40]

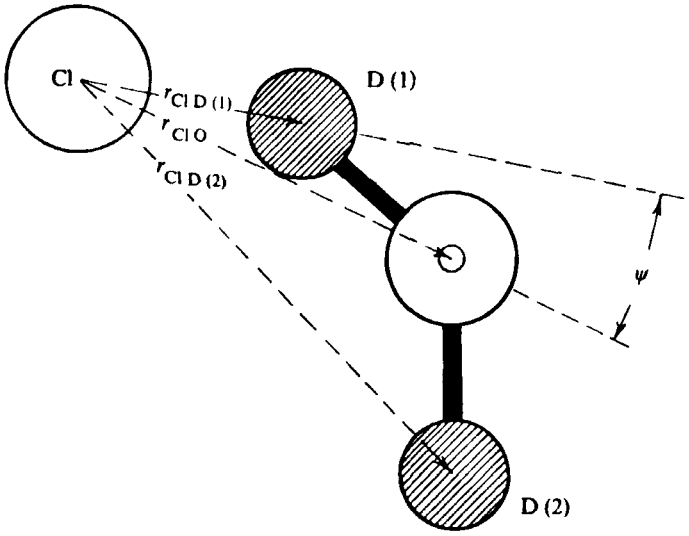

FIGURE 14 The geometry of Cl^- hydration.[38]

Most applications of liquid studies deal with molten metals or alloys or molecular liquids. Enderby and co-workers[37–40] studied chlorides with different counterions in aqueous D_2O solution over the last decade. Aqueous solutions contain four chemical species and so require 10 pair correlation functions. The liquid structure factor can therefore not be extracted from a single experiment. The method proposed to overcome this difficulty is isotopic enrichment, because the scattering length of an atom is a function of the nucleus and varies therefore from one isotope to the next. Figure 13a shows the diffraction pattern for $CaCl_2$ obtained with two different Ca isotopes. The difference between the two patterns is shown in Figure 13b. Further variations of the Cl isotopes and concentration yield the different pair correlations. Data on $NiCl_2$ in D_2O provided clear evidence that the Ni ions are arranged on a quasilattice and possess a substantial degree of long-range order.[37] A series of measurements on alkali and alkali earth chlorides gave some insight into the coordination of the Cl^- ion in D_2O solution (Figure 14).[38] The authors were able to show that the Cl^- hydration is essentially independent of the cation with the possible exception of a transition metal counter ion (Ni^{2+}). The influence of the counterion may therefore

be classified clearly as a second-order effect. There are further indications that the hydration of Ni^{2+} is concentration independent.

DIFFUSION AND ORIENTATION PROCESSES IN SOLIDS

Inelastic incoherent neutron spectra (IINS) are an excellent method for spectroscopic studies on molecules and crystals. Fields of application are diffusion processes, rotation and reorientation of groups of a molecule or crystal field splitting. The large difference in the incoherent scattering of hydrogen and deuterium [cross section $\sigma_{inc}(H)] \approx 80$ b, $\sigma_{inc}(D) \approx 3$ b) is an elegant method to attribute particular energies to a given chemical group. Neutrons yield simultaneously both geometrical and dynamic information. Most of the work concerns incoherent, quasielastic scattering, which gives information about the motion of individual atoms and hence molecules. Three types of motion are distinguished: free rotation, rotational diffusion, jump and reorientation. It should be emphasized that with present limitations of experimental resolution only motions with correlation times shorter than about 10^{-9}s can be studied.

Infrared, Raman and neutron spectroscopy are complementary and have different selection rules which allow a precise attribution of lines and energies. A series of carbonyls has been studied by White and Wright[41–43] by energy gain time-of-flight spectroscopy (0–500 cm^{-1}) and inverted beryllium-filter energy loss spectroscopy. Hydrogen bending modes were observed and the energies for several compounds are shown in Table III.

TABLE III

Data for hydrogen bonding modes for simple hydrido complexes[45]

Compound	cm^{-1}
$HCo(PF_3)_4$	652
$HCo(CO)_4$	696
$H_2Fe(CO)_4$	760/690
$KHFe(CO)_4$	715
$HMn(CO)_5$	730/600
$H_3Mn_3(CO)_{12}$	610
$HFe_3(CO)_{11}$	706

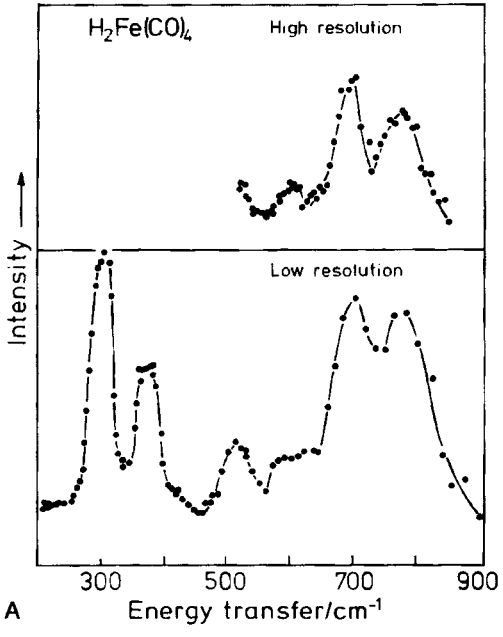

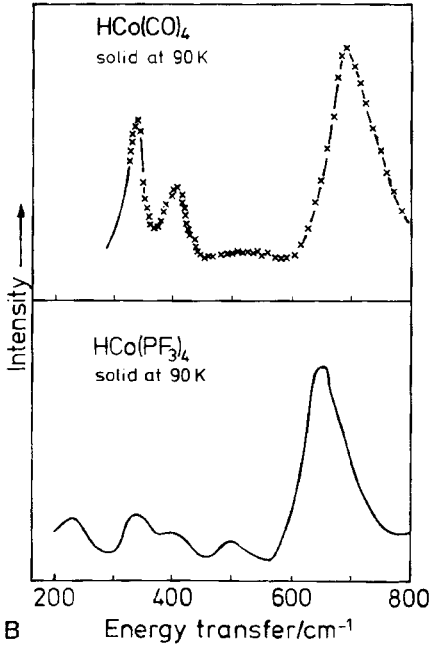

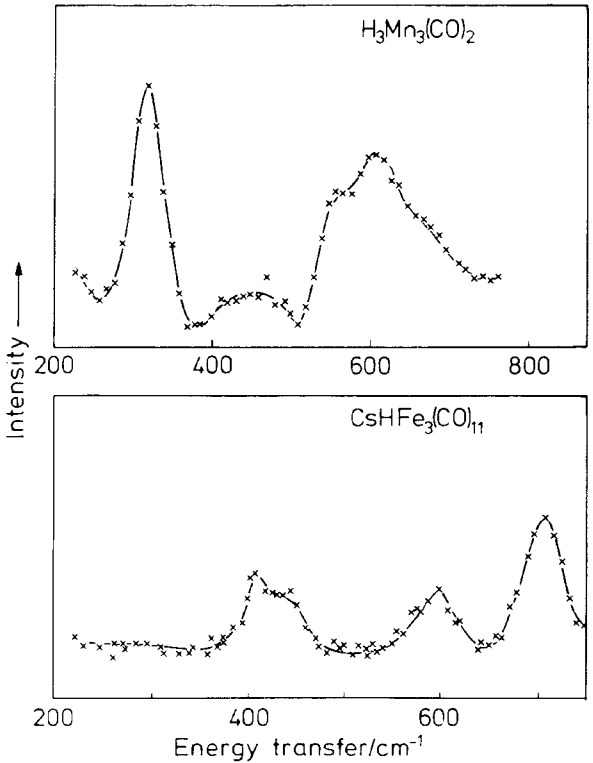

C

FIGURE 15 Inelastic neutron specta of hydridocarbonyls of transition metals.[44]

In $HCo(CO)_4$ and $HCo(PF_3)_4$ the molecular symmetry is C_{3v} and accordingly a single hydrogen bending frequency is observed in the neutron spectrum (Figure 15) at 696 and 652 cm^{-1}, respectively. The assignment of the additional modes was performed by comparison of gas-phase infrared with the neutron spectrum. In $H_2Fe(CO)_4$ the molecular symmetry is C_{2v} and in contrast with the spectrum of $HCo(CO)_4$, a new band with medium intensity appears at 510 cm^{-1}. This is a carbonyl band, which is now neutron active through mixing with the hydrogen band because the symmetry in the iron compound is lower. The $H_3Mn_3(CO)_{12}$ spectrum is similar to that of $H_2Fe(CO)_4$ in the number of bands observed and the overall intensity pattern. From the intensity pattern the bands in the 600 cm^{-1} region can be tentatively assigned to the hydrogen-bending vibrations and in the IINS spectrum of $CsHFe_3(CO)_{11}$ the strongest band can be similarly assigned. Only little displacement of the metal hydrogen bending appears in going from a two-electron, two-center bond to a three-center bond. For manganese a drop of 60 cm^{-1} from $HMn(CO)_5$ to $H_3Mn(CO)_{12}$ is observed. Similar studies were published for hydridocarbonyl systems containing a ring of three metal atoms: $H_3Mn_3(CO)_{12}$, $H_3Re_3(CO)_{12}$, $CsHFe_3(CO)_{11}$.[42] The authors claim that there is little mixing of metal–carbon deformation modes with metal–metal stretching vibrations in metal clusters and that, to a reasonable approximation, the small perturbation introduced by a hydrogen atom sited between two metal atoms has no effect on this external ligand-cluster mixing.

Rotational motion of molecules or parts of molecules is investigated by the observation of the broadening at the bottom of the elastic line in a neutron spectrum. This so-called quasielastic part is due to small energy changes as compared to the incoming neutron beam. Ammonium compounds are a favored group of study due to the relatively compact NH_4^+ group which is connected with neighboring atoms only by hydrogen bonds. Most ammonium compounds, especially the halides, show several phase transitions. The NH_4^+ group in NH_4Br is freely rotating in the high-temperature phase. However, it occupies two positions in phase II ($235.2 \leq T \leq 411.1$ K). The time needed for a reorientation between these distinguishable positions is assumed to be small as compared to the average time τ the rotating group spends at a particular orientation. The temperature dependence of the quasielastic scattering is shown in Figure 16 for NH_4Br as determined by Lechner

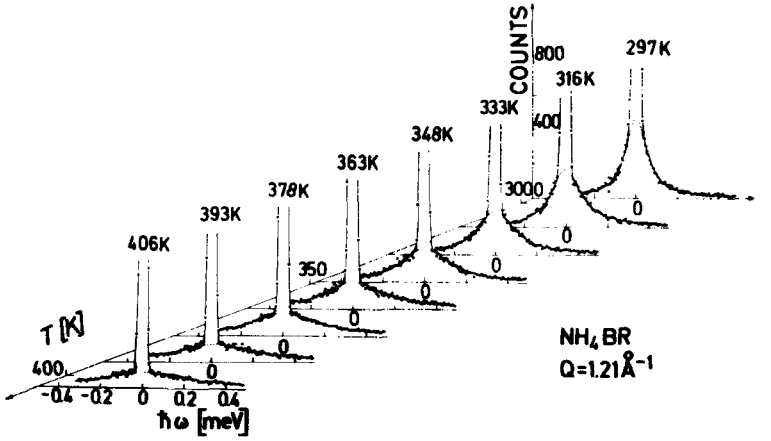

FIGURE 16 Temperature dependence of the quasielastic scattering in NH_4Br. The solid lines are fits of the C_4-rotational jump model to the experimental data.[43]

et al.[44] The experimental data fit well with a jump diffusion model and the authors derived the average time τ as well as the activation energy. The temperature dependence of τ is explicitly stated by an Arrhenius law, but no significant variation of the activation energy as a function of time was found.

Further studies on diffusion processes have been performed for the movement of hydrogen in metals[11,46,47] and for ion mobility in solid electrolytes. The diffusive step may be similar in both classes of compounds. Studies on the superionic conductor α-AgJ with respect to the motion of Ag^+ ions[48,49] indicate similarities to the motion of hydrogen in metals at elevated temperatures.

Acknowledgments

The neutron experiments of our research group are supported by the Bundesministerium für Forschung und Technologie of the Federal Republic, Bonn. Experiments were performed at the FR2 reactor, KFK, Karlsruhe, and the HBFR at the ILL, Grenoble. The author wishes to express his gratitude to these institutions. All new diagrams and some of those reproduced have carefully been drawn by Miss A. Haake and the manuscript

was typed with great care by Mrs. S. Whitehead. Their collaboration is acknowledged with many thanks.

HARTMUT FUESS
Institut für Kristallographie und Mineralogie der Universität Senckenberganlage 30, 6000 Frankfurt am Main 1, Federal Republic of Germany

References

1. G. E. Bacon, *Neutron Diffraction*, 3rd ed. (The Clarendon Press, Oxford, 1975).
2. H. Fuess, in *Modern Physics in Chemistry*, Vol. 2, edited by E. Fluck and V. Goldanskii (Academic Press, London, 1979), pp. 1–193.
3. W. Marshall and S. W. Lovesey, *Theory of Thermal Neutron Scattering* (The Clarendon Press, Oxford, 1971).
4. H. M. Rietveld, J. Appl. Cryst. **2,** 65–71 (1969).
5. A. W. Hewat, Profile Refinement of Neutron Powder Diffraction Patterns, Rapport ILL 74H625/1 (1974).
6. G. S. Pawley, G. A. Mackenzie and O. W. Dietrich, Acta Cryst. A **33,** 142–145 (1977).
7. G. S. Pawley, Faraday Discuss. Chem. Soc. **69,** 157–163 (1980).
8. A. K. Cheetham and J. C. Taylor, J. Solid State Chem. **21,** 253–275 (1977).
9. A. W. Hewat, J. Phys. C. **6,** 1074–1084 (1973).
10. A. W. Hewat, J. Phys. C. **6,** 2559–2572 (1973).
11. T. Springer, in *Dynamics of Solids and Liquids by Neutron Scattering*, Topics in Current Physics 3, edited by Lovesey and Springer (Springer-Verlag, Berlin, 1977), pp. 255–300.
12. M. Ishikawa, Acta Cryst. B **34,** 2074–2080 (1978).
13. R. Bau and T. F. Koetzle, Pure Appl. Chem. **50,** 55–64 (1978).
14. D. W. Hart, R. G. Teller, C. Y. Wei, R. Bau, G. Longoni, S. Campanella, P. Chini and T. F. Koetzle, Angew. Chem. Int. Ed. Engl. **38,** 80 (1979).
15. P. F. Jackson, B. F. G. Johnson, J. Lewis, P. R. Raithby, M. Mapartlin, W. J. H. Nelson, K. D. Rouse, J. Allibon and S. A. Mason, J. Chem. Soc. Chem. Commun. **1980,** 295–297 (1980).
16. R. Bau, W. E. Carroll, R. G. Teller and T. F. Koetzle, J. Am. Chem. Soc. **99,** 3872–3874 (1977).
17. G. E. Bacon, P. J. Bacon and R. K. Griffiths, Proc. Roy. Soc. Lond. D **204,** 355–362 (1979).
18. G. E. Bacon, in *Neutrons in Biology*, edited by D. Worcester (Elsevier, North-Holland, in press).
19. S. W. White, D. J. S. Hulmes, A. Miller and P. A. Timmins, Nature **266,** 421–425 (1977).
20. C. Riekel, Prog. Solid State Chem. **13,** 89–117 (1980).
21. C. Riekel and C. O. Fischer, J. Solid State Chem. **29,** 181–190 (1979).
22. H. B. Stuhrmann and A. Miller, J. Appl. Cryst. **11,** 325–345 (1978).
23. D. Worcester (editor) *Neutrons in Biology* (Elsevier, North-Holland, in press).
24. H. Fuess, J. W. Bats, H. Dannöhl, H. Meyer and A. Schweig, Acta Cryst. B **38,** 736–743 (1982).

25. H. Fuess, N. Burger and J. W. Bats, Z. Kristallogr. **156,** 219–232 (1981).
26. J. O. Thomas, Acta Cryst. A **34,** 819 (1978).
27. J. M. Savariault and M. S. Lehmann, J. Am. Chem. Soc. **102,** 1298–1303 (1980).
28. R. Goddard and C. Krüger, in *Electron Distribution and the Chemical Bond,* edited by P. Coppens (Plenum, New York, 1982).
29. P. J. Brown and J. B. Forsyth, Proc. Phys. Soc. **92,** 125 (1967).
30. V. R. Rakhecha and S. N. Satya Murtly, J. Phys. C **11,** 4389 (1978).
31. M. Bonnet, A. Delapalme, H. Fuess and P. Becker, J. Phys. Chem. Sol. **40,** 863–876 (1979).
32. P. J. Brown, A. Capiomont, B. Gillon and J. Schweizer, J. Magn. Mag. Mat. **14,** 289–294 (1979).
33. J. W. White, in *Dynamics of Solids and Liquids by Neutron Scattering,* Topics in Current Physics, 3, edited by Lovesey and Springer (Springer-Verlag, Berlin, 1977), pp. 197–252.
34. J. K. Kjems, L. Passell, H. Taub, J. G. Dash and A. N. Novaco, Phys. Rev. **13,** 1446 (1976).
35. H. Jobic, J. Tomkinson, J. P. Candy, P. Fouilloux and A. J. Renouprez, Surf. Sci. **95,** 496–510 (1980).
36. P. Chieux, in *Neutron Diffraction,* edited by H. Dachs (Springer-Verlag, Berlin, 1978), pp. 271–301.
37. R. A. Howe, W. S. Howells and J. E. Enderby, J. Phys. C **7,** L111–L114 (1974).
38. S. Cummings, J. E. Enderby, G. W. Neilson, J. R. Newsome, R. A. Howe, W. S. Howells and A. K. Soper, Nature **287,** 714–716 (1980).
39. G. W. Neilson and J. E. Enderby, J. Phys. C **11,** L625 (1978).
40. S. Cummings, J. E. Enderby and R. A. Howe, J. Phys. C **13,** 1–8 (1980).
41. J. W. White and C. J. Wright, J. Chem. Soc. D **920** (1970).
42. J. W. White and C. J. Wright, J. Chem. Soc. A **2843** (1971).
43. J. W. White and C. J. Wright, J. Chem. Soc. Faraday Trans. 2, **68,** 1423 (1972).
44. R. E. Lechner, G. Badurek, A. J. Dianoux, H. Hervet and F. Volino, J. Chem. Phys. **73,** 934–939 (1980).
45. J. Howard and T. C. Waddington, Adv. Infrared Raman Spectrosc., **7,** 86–222 (1980).
46. T. Springer, in *Hydrogen in Metals I,* Topics in Applied Physics 28, edited by G. Alefeld and J. Völkl (Springer-Verlag, Berlin, 1978), pp. 75–98.
47. K. Sköld, in *Hydrogen in Metals I,* Topics in Applied Physics 28, edited by G. Alefeld and J. Völkl (Springer-Verlag, Berlin, 1978), pp. 267–287.
48. K. Funke, Chapter 6 in *Solid Electrolytes,* edited by W. Hagenmüller and W. van Gool (Academic, New York, 1978).
49. K. Funke, A. Höch and R. E. Lechner, J. Phys. Colloq. C **6,** Suppl. 7, **41,** C6–17 (1980).